

Novel technique to deblurring and blur detection techniques for enhanced visual clarity of ancient images

Poonam Pawar, Bharati Ainapure

Department of Computer Engineering, Faculty of Science and Technology, Vishwakarma University, Pune, India

Article Info

Article history:

Received Jun 7, 2024

Revised Oct 4, 2024

Accepted Oct 23, 2024

Keywords:

Ancient images

Convolutional neural networks

Deblur

Degraded images

Wavelet transform

ABSTRACT

Digital image quality often degrades due to various factors such as noise and blur. Many images are affected by these issues, reducing their clarity and accuracy. This degradation is especially problematic for ancient images, significantly hampers the ability to analyze historical documents and artworks. This paper presents a novel approach to both blur detection and deblur ancient images, enhancing their clarity and readability. This research introduces a technique that combines wavelet transform and convolutional neural networks (CNNs) for effective blur identification and deblurring, specifically aimed at restoring blurred ancient images, regardless of the type of blur degradation. This novel approach demonstrated an average accuracy of 98.3% in blur detection on ancient image datasets. The performance of deblurring algorithms is typically evaluated using metrics such as peak signal-to-noise ratio (PSNR), mean squared error (MSE), and structural similarity index (SSIM) which quantify fidelity and quality of the deblurred images. In the deblurring, this approach produced PSNR values of 55.5 to 68.3 dB, MSE values of 2.99 to 11.1, and an SSIM of 0.9 across different types of blurs. These results show significant promise for the restoration of ancient images, providing researchers, historians, and archaeologists with valuable tool for conservation cultural heritage.

This is an open access article under the [CC BY-SA](https://creativecommons.org/licenses/by-sa/4.0/) license.



Corresponding Author:

Bharati Ainapure

Department of Computer Engineering, Faculty of Science and Technology, Vishwakarma University

Pune 411048, Maharashtra, India

Email: bharati.ainapure@vupune.ac.in

1. INTRODUCTION

Images are essential in today's digital world for many applications, from satellite imagery to medical diagnosis [1], [2]. However, their quality often suffers due to factors like noise, blur, and compression artifacts. Thus, image restoration becomes crucial for restoring the original image and enhancing visual quality to provide correct interpretation and analysis [3]. Likewise, an important application of image restoration is in ancient image restoration, where it plays a vital role in mitigating degradation effects in ancient images. As such their preservation is of utmost importance for scholars, historians, and art conservators [4].

Today, effective image restoration relies on accurate blur detection and identification. Deblurring algorithms perform optimally when tailored to the specific type of blur, significantly improving image clarity. By addressing particular degradation issues, blur detection and deblurring play a crucial role in enhancing the overall quality and accuracy of restored images [5]. This process is especially important in the digital restoration of ancient images. It focuses on identifying areas within an image that are blurred, which can result from various factors such as camera movement, focus issues, or environmental conditions during storage. It aids targeted restoration, helping historians better interpret details. High-quality digital versions

preserve cultural treasures for future generations, ensuring historical accuracy and effective digital archiving [6]. Overall, blur detection is vital for preserving and accurately representing historical and cultural heritage.

Accurate detection also serves as a basis for subsequent deblurring processes and is vital for numerous applications, including computer vision, medical imaging, surveillance, and consumer photography [7]. The challenge in image blur detection lies in its multifaceted nature. Blur can manifest in various forms, including motion blur induced by camera or object movement, defocus blur resulting from improper focus settings, or lens aberrations that distort the captured scene. Moreover, images may exhibit a combination of these blur types, further complicating the task of designing robust blur detection methods [8]. Consequently, extensive research has focused on developing diverse techniques to accurately identify and classify blur, utilizing methods such as machine learning, frequency domain analysis and edge detection.

Significant advancements in blur detection technologies have been largely driven by the use of convolutional neural networks. Early techniques, such as those by Vijay [9] utilized convolutional neural networks (CNNs) for general image deblurring, setting a precedent for more targeted approaches. By introducing an ensemble CNN approach with pruned versions of AlexNet and GoogleNet, Wang *et al.* [10] demonstrated a significant enhancement in classifying various blur types compared to traditional methods. Kim *et al.* [11] employed a deep encoder-decoder network with multi-scale features to effectively detect defocus and motion blur. Huang and Xia [5] further advanced the field with a joint method that combines blur kernel estimation with CNN-based deconvolution, significantly improving image restoration quality. Recent evaluations by Pagaduan *et al.* [12] have provided insights into the effectiveness of different blur detection techniques, leading to the development of sophisticated models such as the pyramid m-shaped deep neural network (PM-Net) by Wang *et al.* [13], which enhances both accuracy and speed in blur detection, and the multi-scale dilated U-Net model by Xiao *et al.* [14], which integrates multi-scale features for superior detection performance. ML and neural networks are powerful techniques used for classification tasks used in many applications [15]–[17]

Image deblurring technology has evolved significantly in various imaging applications from image surveillance to medical imaging using recent techniques [18]. Li *et al.* [19] developed a module using the gray level co-occurrence matrix (GLCM) to improve texture preservation in deblurred images, crucial for digital photography and vision systems. Wang *et al.* [20] one-step CNN method further advanced the field by effectively restoring blurry face images, benefiting facial recognition technologies. Peng *et al.* [21] integrated deblurring with feature-based sparse representation, enhancing both image clarity and matching accuracy. Zhang *et al.* [22] combined deblurring with super-resolution through attention dual supervised networks, improving high-resolution imaging, particularly in medical and satellite applications. Finally, Chowdhury *et al.* [23] addressed Poisson noise and blur in scientific imaging with fractional-order total variation regularization, crucial for fields like astronomy and biology. These innovations reflect a trend towards more tailored and effective deblurring solutions across diversified domains.

Blur detection and deblur techniques have made notable advancements in recent years but still grapple with several challenges. Accurate blur detection is challenging due to the varying types and degrees of blur, noise interference, and the presence of textures that might be mistaken for blur. Deblurring research faces challenges such as handling various types of blurs (motion, defocus, and Gaussian), accurately estimating non-uniform blur kernels, and balancing computational complexity with artifact suppression. Additionally, deep learning approaches bring issues like the need for large training datasets and ensuring model generalization across diverse real-world conditions.

This research focuses on following objectives: i) developing more robust and generalized models that can handle diverse types of blurs, ii) reducing computational complexity to enable real-time applications such ancient image restoration, iii) combining blur detection and deblurring into a single unified framework for more efficient processing, and iv) exploring the use of new architectures and training techniques in deep learning to further enhance performance. This paper is organized as follows: the introduction is given in section 1, the suggested methodology is described in section 2, and the experimental setup, results, and discussion are presented in section 3. Finally, the conclusion is provided in section 4.

2. METHOD

Restoring ancient images is vital for preserving our shared cultural heritage, offering glimpses into the past, and enriching our understanding of history. Figure 1 outlines the flow of the blur detection and deblurring technique. The “Historical places dataset of Pune” is used as the ancient image dataset for this approach. The dataset spans various categories as “Omkareshwar Mandir,” “Shaniwar Wada,” “Kasaba Ganapati Mandir,” “Parvati,” “Lal Mahal,” and “Tulashibaug Ram Mandir” [24]. This dataset generates degraded images for model building by adding various types of blurs. These degraded images undergo multiple levels of image degradation detection, including preprocessing, feature extraction, and neural network classification. Then identified type of blur utilized for the subsequent deblurring process to restore

the images. Finally, performance analysis is conducted using peak signal-to-noise ratio (PSNR), mean squared error (MSE), and structural similarity index (SSIM) metrics.

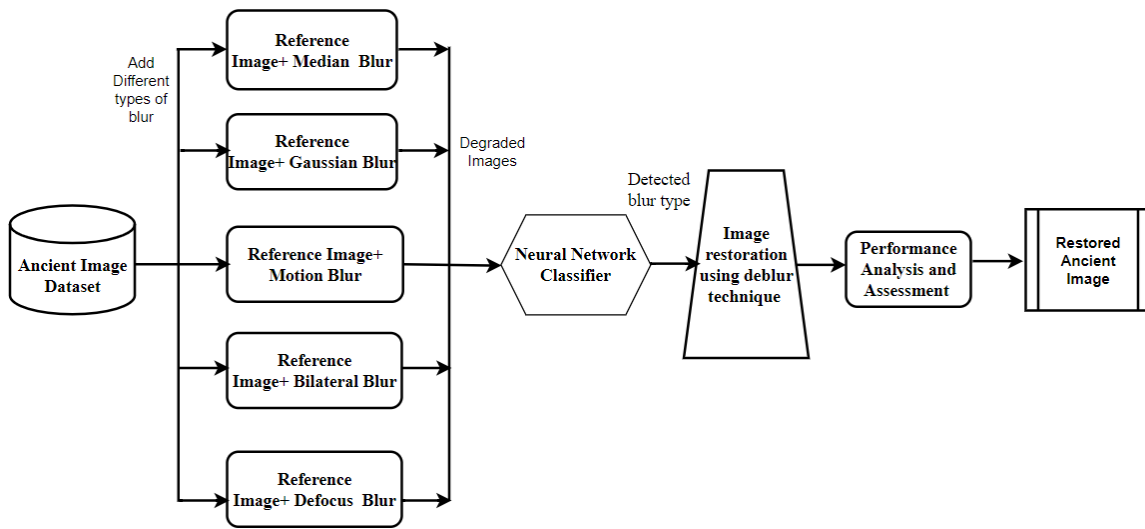


Figure 1. Flow for blur detection and deblur process

2.1. Architecture for blur identification

The architecture for blur identification, illustrated in Figure 2, determines the specific degradation type and facilitates the restoration of degraded images accordingly. A degraded image is input for this identification process which is generated through mixing blur in the original image. Feature extraction, especially using wavelet transform, is crucial in neural networks as it reduces data dimensionality and captures important pattern. This approach boosts the network's efficiency, accuracy, and generalization by focusing on the most relevant features. The wavelet transform is commonly employed for feature extraction, with resulting features then fed into a neural network for classification.

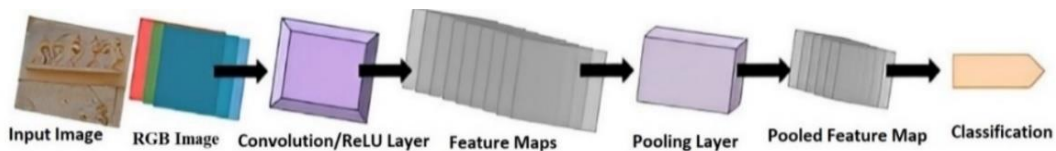


Figure 2. Blur identification architecture

Further, these extracted features are processed through the convolution/rectified linear unit (ReLU) layer of CNN. The main aim of the convolution/ReLU layer is to introduce the non-linearity and to solve the issue related to the vanishing gradient. Here, we have considered the negative values also with a negative slope to it.

The PReLU function is as given in (1).

$$PReLU(k) = \max(0, k) + M \times \min(0, k) \tag{1}$$

where M is the learnable parameter and k is the feature values. The parameter M learns by using back propagation at a negligible increase in the cost of training.

$$L_{\delta}(y, f(x)) = \begin{cases} \frac{1}{2}(y-f(x))^2 & \text{for } |y-f(x)| \leq \delta, \\ \delta|y-f(x)| - \frac{1}{2}\delta^2 & \text{otherwise} \end{cases} \tag{2}$$

where L_δ is the backpropagation function that depends on y and $f(x)$. δ (delta) is the small amount of change that occurred in the weight's adjustment. y is the changes in weights that tracked in the forward direction. $f(x)$ is the changes in weights that tracked in the backward direction.

The equation consolidates MSE and MAE with dependency on another parameter called delta. If the delta is high, the loss function works as an MSE; if the delta is low, then the loss function works as an MAE. As the final outcome the CNN determines whether the degraded image is affected by defocus, bilateral, gaussian, median, or motion blur.

2.2. Architecture for deblur technique

After detecting the type of blur next process starts for the deblur technique. The deblur architecture is shown in Figure 3. The approach of patch extraction and non-linear mapping for restoration and detailing involves several key steps aimed at enhancing the quality and fidelity of images. Firstly, patch extraction involves dividing the input image into smaller, overlapping regions or patches. This process allows for a more localized analysis and manipulation of image features, facilitating targeted restoration and detailing. Following patch extraction, a non-linear mapping technique is applied to each patch. Non-linear mapping methods enable more sophisticated transformations of pixel values, allowing for the enhancement of image details and restoration of lost information. These mappings often involve complex mathematical functions that effectively adjust pixel values based on local image characteristics.

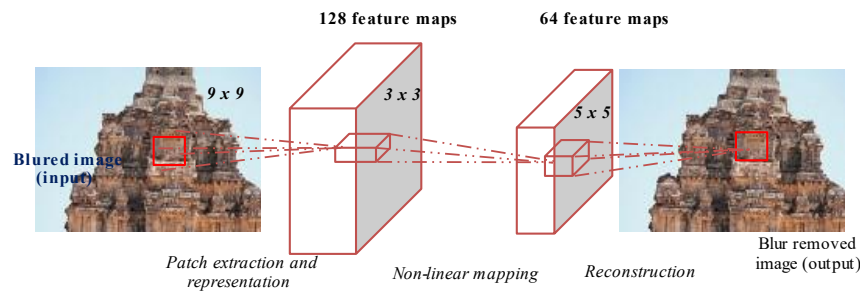


Figure 3. Deblur architecture

2.2.1. Patch extraction

The initial phase employs 128 filters sized $9 \times 9 \times 3$ for the window's patch extraction. It processes extracted image patches X using 128 filters $W1$ and biases $B1$. The selection of these weights $W1$ is adapted based on the type of blur identified in the initial stage, allowing the neural network to focus on specific blur characteristics within localized patches. This approach improves the network's ability to differentiate between blurred and sharp regions, leading to more accurate predictions. The expression for the neural network's first layer is defined as (3):

$$F1(X) = W1 \times X + B1 \quad (3)$$

where X denotes the image, $W1$ represents the 128 filters utilized, and $B1$ represents the applied biases.

2.2.2. Non-linear mapping

The feature maps obtained earlier underwent a ReLU activation function. To enhance their resolution, 64 filters of size $64 \times 3 \times 3$ were employed for mapping these activations from ReLU to a higher-dimensional space. This process effectively increases the network's capacity to represent more complex patterns and finer details within the image patches. ReLU activation was applied to ensure non-linearity in this mapping process. This can be represented as (4):

$$F2(X) = \max(0, W2 \times F1(X) + B2) \quad (4)$$

where X represents the image, $W2$ denotes the 64 filters utilized, and $B2$ represents the biases applied.

2.2.3. Restoration

The high restoration underwent three filters, each with a size of 5×5 , to aggregate the restoration mappings in the previous layer. This was a linear mapping and can be represented as (5):

$$F(X) = W3 \times F2(X) + B3 \quad (5)$$

where X represents the image, W3 represents the filters utilized, and B3 represents the biases applied.

3. RESULTS AND DISCUSSION

This section presents the results of the proposed system. The hardware configuration includes an 11th Generation Intel(R) Core (TM) i7-1165G7 @ 2.80 GHz processor with 16 GB of RAM, running on a 64-bit operating system. Coding is performed using Microsoft Visual Studio Code version 1.70.1, in combination with Python 3.6.3. The neural network is executed using TensorFlow and Keras, while image processing tasks are handled by OpenCV.

3.1. Blur type identification performance measures

The confusion matrix is essential for evaluating and improving blur detection algorithms, offering insights into performance metrics and specific errors to guide model refinement. For our system the confusion matrix shows that the classification model performs well, accurately identifying most instances of each blur type. Out of 200 samples for each class, the model correctly classifies the vast majority, with only a few misclassifications in each category. This indicates that the model has a high level of accuracy in distinguishing between motion blur, bilateral blur, gaussian blur, median blur, and defocus blur, as given in Figure 4.

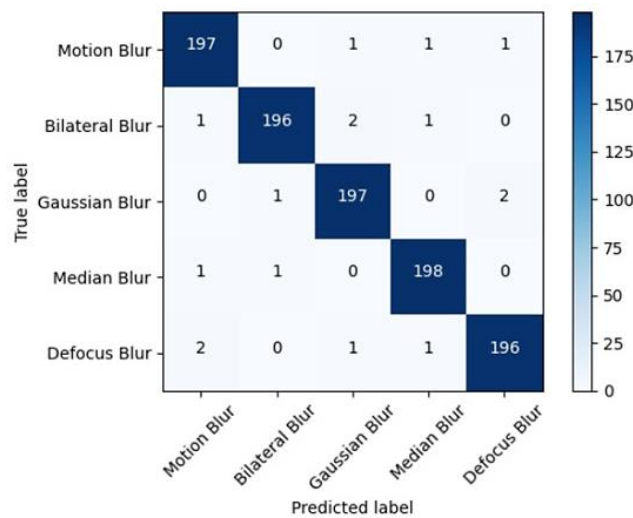


Figure 4. Confusion matrix of different blur types classification

Based on the confusion matrix; the performance parameters have been calculated. The evaluation of blur type identification was thorough, incorporating key performance metrics such as accuracy, precision, recall, and F1-score. Our system demonstrated an impressive overall accuracy of 98.13%. Detailed assessments for each blur type revealed strong performance across all metrics. Accuracy, precision, recall, and F1-score for motion blur achieved 98.88%, 0.98, 0.97, and 0.98, respectively. Similarly, bilateral blur recorded 99.38%, 0.98, 0.99, and 0.99, while gaussian blur matched motion blur with 98.88%, 0.98, 0.97, and 0.98. median blur showed slightly higher values at 99.13%, 0.97, 0.99, and 0.98, and defocus blur achieved 98.01%, 0.97, 0.96, and 0.98, respectively as shown in Table 1.

Table 1. Performance measures using our system

Class	Accuracy	Precision	Recall	F1-score
Motion blur	98.88%	0.98	0.97	0.98
Bilateral blur	99.38%	0.98	0.99	0.99
Gaussian blur	98.88%	0.98	0.97	0.98
Median blur	99.13%	0.97	0.99	0.98
Defocus blur	98.01%	0.97	0.96	0.98

Table 2 presents a comparative overview of various blur identification techniques, datasets, and performance metrics. It features methods like deep neural networks, wavelet transforms, and CNNs applied to datasets such as blur detection dataset (BDD), challenging defocused dataset (CDD), and VOC 2012. The metrics indicate strong performance, with values ranging from 85.68% to 100%. Significantly, the proposed system achieves 98% accuracy on ancient image datasets by utilizing a combination of wavelet transform and CNN.

Table 2. Comparative study of blur identification technique

Paper	Image/dataset	Types of blurs	Technique	Performance metrics
[13]	BDD and CDD	Motion or defocus blur	End-to-end deep neural network. pyramid ensemble model (PM-Net) composed of several M-shaped convolutional neural networks	Precision, recall, F1, MAE of U-net is 0.806, 0.780, 0.760, 0.191 of M-shaped Network is 0.841, 0.919, 0.873, 0.104
[25]	Flickr dataset, ILSVRC dataset	Motion or defocus blur	CNNs to learn powerful features relevant to blur	Accuracy 85.68%
[26]	The Oxford building dataset, Caltech 101 dataset, Berkeley dataset and Pascal VOC 2007 dataset.	Defocus, gaussian, haze and motion blur.	Simplified-Fast-AlexNet (SFA)	Accuracy 96.99%
[27]	Bar code image	Motion, defocus, joint blur	Wavelet transform, feed forward neural network	Accuracy of motion, defocus, Joint blur classification is 99.3, 99.7 and 100 respectively
[28]	INRIA aerial image dataset, Caltech-256 Object Category, INRIA Holidays LabelMe, manually select 3789 unblurred high resolution images from four datasets	Gaussian or linear motion blur	Haar wavelet transform	Accuracy, precision, and recall more than 90%
[29]	VOC 2012 dataset	Defocus and motion blur	Deep defocus and object motion blur segmentation	Average precision 0.976
[30]	Author's personal pictures	All	CNN and Laplacian	Accuracy 91%
[31]	SHI and DUT datasets	Motion and defocus blur	Multi sequential deviated patterns (MSDPs)	Precision, Recall, F1-score of Shi dataset 0.91, 0.90, 0.92 and of DUT dataset is 0.89, 1 0.91, 0.88
Our System	Ancient images like historical places near Pune city	Motion blur, bilateral blur, gaussian blur, median blur, defocus blur	Wavelet transform and CNN	Accuracy, precision, F1-score and recall is above 98%, 0.97, 0.96, 0.98 respectively

The performance of blur type identification was also assessed based different parameters. One aspect of the analysis focuses on the number of hidden layers, showing that using 9 hidden layers produced the best results, as illustrated in Figure 5. The findings reveal that accuracy steadily increases with the addition of hidden layers. However, once the number of hidden layers exceeds 9, a decrease in accuracy is observed.

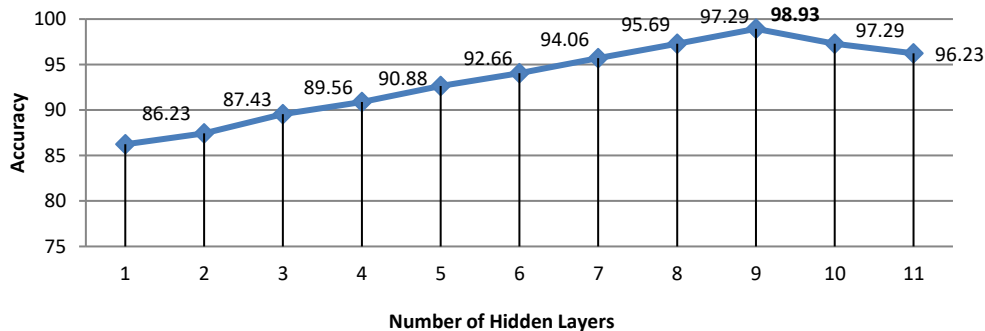


Figure 5. Accuracy for different number of hidden layers

Support vector machine (SVM), random forest (RF), single-layered neural network (single-layered NN), deep neural network (DNN), AlexNet, slow feature analysis (SFA), and are different machine learning models/algorithms used for tasks like image classification, pattern recognition, and regression. Additionally, when comparing our system's performance with other methods such as AlexNet, SFA, random forest, DNN, SVM, and single-layered NN, our system demonstrates superior accuracy, as illustrated in Figure 6. This advantage is particularly notable in complex image recognition tasks, where our system consistently outperforms alternative techniques. The robustness of our approach is evident across various benchmarks underscoring its effectiveness in achieving high levels of accuracy in blur detection and analysis tasks.

Table 3 shows the space complexity for blur classification across different image sizes, with corresponding memory requirements for each. As the image size increases from 250 to 2,000 kB, the memory needed also increases, ranging from 32 to 167 kB. This demonstrates the proportional relationship between image size and memory consumption, underscoring the need for efficient resource management as image sizes grow.

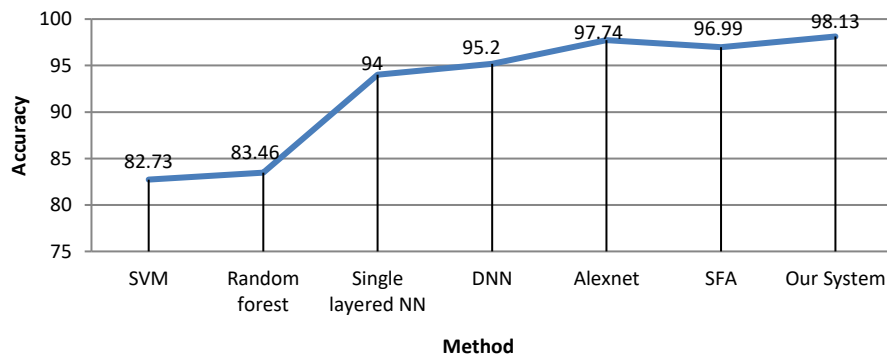


Figure 6. Accuracy of different blur identification methods

Table 3. The space complexity for blur classification for different image sizes

Image size (kB)	Memory requirement (kB)
250	32
500	39
750	53
1,000	78
1,250	109
1,500	132
1,750	149
2,000	167

3.2. Performance measures for deblur technique

PSNR, MSE, and SSIM are widely used metrics for assessing image quality. To assess the fidelity and perceptual quality of the processed content, they are often used in image processing, compression, and restoration. These metrics are used to measure the quality of images by comparing original version to a processed or degraded one. PSNR and MSE focus on pixel-wise differences, while SSIM takes into account structural and perceptual aspects of the images. The choice of which metric to use may depend on the specific goals of the image processing task [32]–[34].

The performance of our system was assessed using PSNR, MSE, and SSIM metrics as presented in Table 4. The results show that the motion blur sample achieved the highest PSNR of 68.3, the lowest MSE of 2.99, and an SSIM of 0.999. The defocus blur sample recorded a PSNR of 65.74, an MSE of 3.89, and an SSIM of 0.996. For the Gaussian blur sample, the PSNR was 59.85, MSE was 7.12, and SSIM was 0.994. The median blur sample had a PSNR of 58.59, an MSE of 8.09, and an SSIM of 0.996. Lastly, the bilateral blur sample had the lowest PSNR at 55.5, an MSE of 11.1, and an SSIM of 0.993.

Our system's time complexity was tested on various hardware platforms. The results showed that with an i3 CPU and 8 GB RAM, it took 403 milliseconds, while an i5 CPU reduced this to 395 milliseconds, and an i7 CPU further decreased it to 369 milliseconds. The fastest result was achieved with an NVIDIA K80 GPU and 12 GB RAM, taking only 3 milliseconds as shown in Table 5 [35].

Table 4. PSNR, MSE, and SSIM values using our system

Image	PSNR	MSE	SSIM
Bilateral blur sample	55.5	11.1	0.993
Defocus blur sample	65.74	3.89	0.996
Gaussian Blur sample	59.85	7.12	0.994
Median Blur sample	58.59	8.09	0.996
Motion Blur sample	68.3	2.99	0.999

Table 5. Time required for different configurations

Platform			Time required to get a result (in milliseconds)
CPU/GPU	Processor	RAM	
CPU	i3	8GB	403
CPU	i5	8GB	395
CPU	i7	8GB	369
GPU	Nvidia K80	12 GB	003

Figures 7(a) to 7(d) offer a visual representation of our deblurring algorithm's performance by presenting sample results before and after the restoration process. The Figures 7(a) and 7(c) depict the sample blurred input images before deblurring, while the Figures 7(b) and 7(d) show the enhanced, deblurred versions after deblurring process. These images provide a tangible representation of the efficacy of our deblurring algorithm, demonstrating the significant improvement in image quality and clarity achieved through the restoration process.

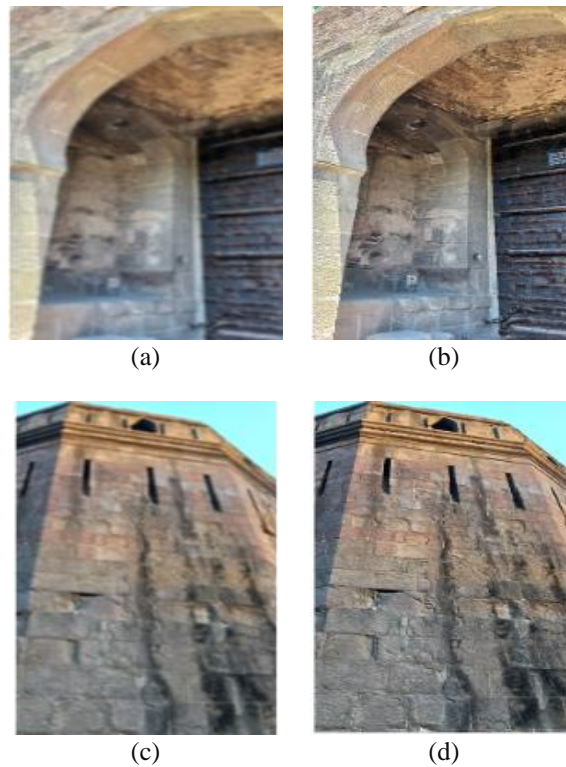


Figure 7. Sample images before deblur and after deblur technique (a) image before deblur, (b) image after deblur, (c) image before deblur, and (d) image after deblur

Table 6 offers an in-depth comparison of deblurring performance, meticulously evaluating our system against alternative techniques. Through meticulous evaluation, our system emerges as the frontrunner, showcasing superior performance metrics when compared to alternative methods. These findings underscore the effectiveness and reliability of our approach in achieving high-quality deblurring results as PSNR value 68.3 dB, MSE value 2.99 and SSIM value 0.999.

Table 6. Deblur performance comparative analysis

Paper Title	Year	Technique	Dataset	PSNR (dB)	MSE	SSIM
“Hierarchical integration diffusion model for realistic image deblurring” [36]	2023	Hierarchical integration diffusion model	GoPro, HIDE, RealBlur a RWBI dataset	36.28	-----	0.96
“Deep multi-scale convolutional neural network for dynamic scene deblurring” [37]	2017	Multi-scale CNN	GoPro, Kohler dataset and own dataset	24.64	-----	0.84
“Learning to see in the dark”[38]	2018	Pipeline	See-in-the-dark (SID) dataset	28.88	----	0.81
“DeblurGAN: blind motion deblurring using conditional adversarial networks” [39]	2017	Generative adversarial networks (GAN)	GoPro dataset and Kohler dataset	28.7	-----	0.958
“Deep generative filter for motion deblurring” [40]	2017	Generative adversarial network	GoPro dataset	28.94	-----	0.9220
“DeblurGAN-v2: deblurring (orders-of-magnitude) faster and better” [41]	2018	Generative adversarial network	GoPro and DVD dataset	29.5	-----	0.93
“Deblurring by realistic blurring” [42]	2020	BGAN and DBGAN	GoPro and RWBI Dataset	31.10	-----	0.94
Our system	2024	Patch extraction, non-linear mapping and restoration	Historical places dataset of Pune	68.3	2.99	0.999

4. CONCLUSION

This research reveals a major advancement in historical image restoration through a system that effectively identifies and classifies blur types in ancient images, achieving an impressive accuracy of 98.13%. Deblur results evaluated using key metrics such as PSNR, MSE, and SSIM, the system exhibits outstanding performance, with PSNR values exceeding 55 dB, MSE as low as 2.99, and SSIM values of 0.9. These metrics are essential for ensuring the high quality and accuracy of restored images, which significantly benefits historical research by providing clearer and more detailed visuals of historical artifacts. Moreover, the system enhances preservation efforts by facilitating better maintenance and restoration of cultural heritage. Its practical applications extend to art conservation and archival work, where improved image clarity supports more accurate documentation, analysis, and preservation of valuable artifacts. However, challenges remain, such as the difficulty in reconstructing severely blurred images and addressing other degradations like noise and physical damage. Future research should focus on developing techniques to handle denoising and improve computational efficiency.

ACKNOWLEDGEMENTS




We are grateful to Vishwakarma University for providing the necessary resources and conducive environment for conducting this research. The support from the faculty and staff has been exceptional.

REFERENCES




- [1] L. Chen, P. Bentley, K. Mori, K. Misawa, M. Fujiwara, and D. Rueckert, “Self-supervised learning for medical image analysis using image context restoration,” *Medical Image Analysis*, vol. 58, 2019, doi: 10.1016/j.media.2019.101539.
- [2] B. S. Ainapure, R. Pise, A. Anil Wagh, J. Tejnani, and K. Oza, “Prognosis of COVID- 19 patients with machine learning techniques,” *Annals of the Romanian Society for Cell Biology*, vol. 25, no. 6, pp. 20183–20200, 2021.
- [3] P. Pawar and B. Ainapure, “Discover image restoration: analysis and novel architecture proposal,” in *7th International Conference on Inventive Computation Technologies, ICICT 2024*, 2024, pp. 622–628, doi: 10.1109/ICICT60155.2024.10544568.
- [4] Y. Zeng, Y. Gong, and X. Zeng, “Controllable digital restoration of ancient paintings using convolutional neural network and nearest neighbor,” *Pattern Recognition Letters*, vol. 133, pp. 158–164, 2020, doi: 10.1016/j.patrec.2020.02.033.
- [5] L. Huang and Y. Xia, “Joint blur kernel estimation and CNN for blind image restoration,” *Neurocomputing*, vol. 396, pp. 324–345, 2020, doi: 10.1016/j.neucom.2018.12.083.
- [6] J. Cao, Y. Jia, M. Yan, and X. Tian, “Superresolution reconstruction method for ancient murals based on the stable enhanced generative adversarial network,” *Eurasip Journal on Image and Video Processing*, vol. 2021, no. 1, 2021, doi: 10.1186/s13640-021-00569-z.
- [7] I. Aizenberg, T. Bregin, C. Butakoff, V. Karnaukhov, N. Merzlyakov, and O. Milukova, “Type of blur and blur parameters identification using neural network and its application to image restoration,” in *Lecture Notes in Computer Science (including subseries Lecture Notes in Artificial Intelligence and Lecture Notes in Bioinformatics)*, vol. 2415, 2002, pp. 1231–1236, doi: 10.1007/3-540-46084-5_199.
- [8] K. Zhang *et al.*, “Deep image deblurring: a survey,” *International Journal of Computer Vision*, vol. 130, no. 9, pp. 2103–2130, 2022, doi: 10.1007/s11263-022-01633-5.
- [9] R. V. J. Vijay, “Image deblurring using convolutional neural network,” *IOSR Journal of Electronics and Communication Engineering Ver. II*, vol. 11, no. 5, pp. 2278–2834, 2016, doi: 10.9790/2834-1105020712.

- [10] R. Wang, W. Li, and L. Zhang, "Blur image identification with ensemble convolution neural networks," *Signal Processing*, vol. 155, pp. 73–82, 2019, doi: 10.1016/j.sigpro.2018.09.027.
- [11] B. Kim, H. Son, S. J. Park, S. Cho, and S. Lee, "Defocus and motion blur detection with deep contextual features," *Computer Graphics Forum*, vol. 37, no. 7, pp. 277–288, 2018, doi: 10.1111/cgf.13567.
- [12] R. A. Pagaduan, M. C. R. Aragon, and R. P. Medina, "iBlurDetect: image blur detection techniques assessment and evaluation study," in *Proceedings of the International Conference on Culture Heritage, Education, Sustainable Tourism, and Innovation Technologies*, 2020, pp. 286–291, doi: 10.5220/0010307702860291.
- [13] X. Wang, S. Zhang, X. Liang, H. Zhou, J. Zheng, and M. Sun, "Accurate and fast blur detection using a pyramid m-shaped deep neural network," *IEEE Access*, vol. 7, pp. 86611–86624, 2019, doi: 10.1109/ACCESS.2019.2926747.
- [14] X. Xiao, F. Yang, and A. Sadovnik, "MSDU-Net: A multi-scale dilated u-net for blur detection," *Sensors*, vol. 21, no. 5, pp. 1–13, Mar. 2021, doi: 10.3390/s21051873.
- [15] J. Wu and C. Hicks, "Breast cancer type classification using machine learning," *Journal of Personalized Medicine*, vol. 11, no. 2, pp. 1–12, Jan. 2021, doi: 10.3390/jpm11020061.
- [16] A. S. Ladkat *et al.*, "Deep neural network-based novel mathematical model for 3D brain tumor segmentation," *Computational Intelligence and Neuroscience*, vol. 2022, pp. 1–8, Aug. 2022, doi: 10.1155/2022/4271711.
- [17] P. Pawar, B. Ainapure, M. Rashid, N. Ahmad, A. Alotaibi, and S. S. Alshamrani, "Deep learning approach for the detection of noise type in ancient images," *Sustainability*, vol. 14, no. 18, pp. 1–19, Sep. 2022, doi: 10.3390/su14181786.
- [18] B. S. Ainapure and P. Y. Pawar, "Image restoration using recent techniques: a survey," *Design Engineering*, vol. 2021, no. 7, pp. 13050–13062, Sep. 2021, doi: 10.17762/de.vi.4560.
- [19] L. Li, Y. Yan, Y. Fang, S. Wang, L. Tang, and J. Qian, "Perceptual quality evaluation for image defocus deblurring," *Signal Processing: Image Communication*, vol. 48, pp. 81–91, 2016, doi: 10.1016/j.image.2016.09.005.
- [20] L. Wang, Y. Li, and S. Wang, "DeepDeblur: Fast one-step blurry face images restoration," *arXiv:1711.09515*, Nov. 2017.
- [21] J. Peng, Y. Shao, N. Sang, and C. Gao, "Joint image deblurring and matching with feature-based sparse representation prior," *Pattern Recognition*, vol. 103, 2020, doi: 10.1016/j.patcog.2020.107300.
- [22] D. Zhang, Z. Liang, and J. Shao, "Joint image deblurring and super-resolution with attention dual supervised network," *Neurocomputing*, vol. 412, pp. 187–196, 2020, doi: 10.1016/j.neucom.2020.05.069.
- [23] M. R. Chowdhury, J. Qin, and Y. Lou, "Non-blind and blind deconvolution under Poisson noise using fractional-order total variation," *Journal of Mathematical Imaging and Vision*, vol. 62, no. 9, pp. 1238–1255, 2020, doi: 10.1007/s10851-020-00987-0.
- [24] P. Y. Pawar and B. S. Ainapure, "Image dataset of Pune city historical places for degradation detection, classification, and restoration," *Data in Brief*, vol. 51, 2023, doi: 10.1016/j.dib.2023.109794.
- [25] K. Purohit, A. B. Shah, and A. N. Rajagopalan, "Learning based single image blur detection and segmentation," in *2018 25th IEEE International Conference on Image Processing (ICIP)*, Oct. 2018, pp. 2202–2206, doi: 10.1109/ICIP.2018.8451765.
- [26] R. Wang, W. Li, R. Qin, and J. Z. Wu, "Blur image classification based on deep learning," in *IST 2017 - IEEE International Conference on Imaging Systems and Techniques, Proceedings*, 2017, pp. 1–6, doi: 10.1109/IST.2017.8261503.
- [27] S. Tiwari, V. P. Shukla, S. R. Biradar, and A. K. Singh, "Blur classification using wavelet transform and feed forward neural network," *International Journal of Modern Education and Computer Science*, vol. 6, no. 4, pp. 16–23, 2014, doi: 10.5815/ijmecs.2014.04.03.
- [28] G. S. Tran, T. P. Nghiem, and J. C. Burie, "Fast parallel blur detection on GPU," *Journal of Real-Time Image Processing*, vol. 17, no. 4, pp. 903–913, 2020, doi: 10.1007/s11554-018-0837-1.
- [29] A. Alvarez-Gila, A. Galdran, E. Garrote, and J. van de Weijer, "Self-supervised blur detection from synthetically blurred scenes," *Image and Vision Computing*, vol. 92, 2019, doi: 10.1016/j.imavis.2019.08.008.
- [30] T. Szandala, "Convolutional neural network for blur images detection as an alternative for Laplacian method," in *2020 IEEE Symposium Series on Computational Intelligence, SSCI 2020*, 2020, pp. 2901–2904, doi: 10.1109/SSCI47803.2020.9308594.
- [31] A. Khan, A. Javed, A. Irtaza, and M. T. Mahmood, "A robust approach for blur and sharp regions' detection using multisequential deviated patterns," *International Journal of Optics*, vol. 2021, 2021, doi: 10.1155/2021/2785225.
- [32] U. Sara, M. Akter, and M. S. Uddin, "Image quality assessment through FSIM, SSIM, MSE and PSNR—A comparative study," *Journal of Computer and Communications*, vol. 7, no. 3, pp. 8–18, 2019, doi: 10.4236/jcc.2019.73002.
- [33] J. Wang, N. Zheng, B. Chen, and J. C. Principe, "Associations among image assessments as cost functions in linear decomposition: MSE, SSIM, and correlation coefficient," *arXiv:1708.01541*, pp. 1–11, 2017.
- [34] R. Padmapriya and A. Jeyasekar, "Blind image quality assessment with image denoising: a survey," *Journal of Pharmaceutical Negative Results*, vol. 13, no. 3, pp. 386–392, 2022, doi: 10.47750/pnr.2022.13.s03.064.
- [35] A. S. Ladkat, A. A. Date, and S. S. Inamdar, "Development and comparison of serial and parallel image processing algorithms," in *2016 International Conference on Inventive Computation Technologies (ICICT)*, Aug. 2016, vol. 2, pp. 1–4, doi: 10.1109/INVENTIVE.2016.7824894.
- [36] Z. Chen *et al.*, "Hierarchical integration diffusion model for realistic image deblurring," in *Advances in Neural Information Processing Systems 36 (NeurIPS 2023)*, 2023, vol. 36, pp. 1–12.
- [37] S. Nah, T. H. Kim, and K. M. Lee, "Deep multi-scale convolutional neural network for dynamic scene deblurring," *Proceedings - 30th IEEE Conference on Computer Vision and Pattern Recognition, CVPR 2017*, vol. 2017-Janua, pp. 257–265, 2017, doi: 10.1109/CVPR.2017.35.
- [38] C. Chen, Q. Chen, J. Xu, and V. Koltun, "Learning to see in the dark," in *Proceedings of the IEEE Computer Society Conference on Computer Vision and Pattern Recognition*, 2018, pp. 3291–3300, doi: 10.1109/CVPR.2018.00347.
- [39] O. Kupyn, V. Budzan, M. Mykhailych, D. Mishkin, and J. Matas, "DeblurGAN: blind motion deblurring using conditional adversarial networks," in *Proceedings of the IEEE Computer Society Conference on Computer Vision and Pattern Recognition*, 2018, pp. 8183–8192, doi: 10.1109/CVPR.2018.00854.
- [40] S. Ramakrishnan, S. Pachori, A. Gangopadhyay, and S. Raman, "Deep generative filter for motion deblurring," in *2017 IEEE International Conference on Computer Vision Workshops (ICCVW)*, Oct. 2017, pp. 2993–3000, doi: 10.1109/ICCVW.2017.353.
- [41] O. Kupyn, T. Martyniuk, J. Wu, and Z. Wang, "DeblurGAN-v2: deblurring (orders-of-magnitude) faster and better," in *Proceedings of the IEEE International Conference on Computer Vision*, 2019, pp. 8877–8886, doi: 10.1109/ICCV.2019.00897.
- [42] K. Zhang *et al.*, "Deblurring by Realistic Blurring," in *Proceedings of the IEEE Computer Society Conference on Computer Vision and Pattern Recognition*, 2020, pp. 2734–2743, doi: 10.1109/CVPR42600.2020.00281.

BIOGRAPHIES OF AUTHORS

Poonam Pawar    has completed B.E. in information technology and M.E. in computer engineering from Savitribai Phule Pune University, Pune. Currently she is pursuing her Ph.D. at Vishwakarma University in Computer Engineering Department. She is an assistant professor of Information Technology at the Savitribai Phule Pune University, Pune. She has more than 19 years of experience in teaching. She has published more than 20 research papers in international journals and conferences. Her research interest includes computer networks, image processing, machine learning and deep learning. She can be contacted at email: poonam.pawar-315@vupune.ac.in and poonam.y.pawar@gmail.com.



Bharati Ainapure    has completed B.E. in computer science and engineering from Karnataka University and M.Tech. in computer science and engineering from Vishweshryaya Technological University, Kanataka, in 2008. She did her Ph.D. from JNTU, Anapatur, India. Currently, she is working as associate professor in Computer Engineering Department, Vishwakarma University, Pune, India. She has more than 26 years of experience in teaching and industry and has published more than 40 research papers in renowned international journals and conferences. She holds six international and national patents in her name. Her research interests include cloud computing, parallel computing, machine learning, deep learning and high-performance computing. She can be contacted at email: bharati.ainapure@vupune.ac.in.